Self-Actuated Microfluidic Chiplet for Two-Stage Multiplex Nucleic Acid Amplification Assay

Supplemental Information

Felix Ansah [a,b], Marziyeh Hajialyani [a], Fatemeh Ahmadi [a], Yuming Gu [a], Ergün Alperay Tarım [a], Michael Mauk [a], Gordon A. Awandare [b], and Haim H. Bau [a,*]

[a] Department of Mechanical Engineering and Applied Mechanics, University of Pennsylvania, Philadelphia, Pennsylvania 19104, United States.

[b] West African Centre for Cell Biology of Infectious Pathogens (WACCBIP), College of Basic and Applied Sciences, University of Ghana, Legon, Ghana.

* Corresponding author: Department of Mechanical Engineering and Applied Mechanics, University of Pennsylvania, 233 Towne Building, Philadelphia, PA 19104. Fax +215-573-6334; e-mail: bau@seas.upenn.edu.

List of Sections, Tables, and Figures

Videos

Video S1: **Penn RAMP Chiplet Operation**. This video describes the chiplet's sequence of operations. The video was recorded with a Google Pixel 7 smartphone camera at 60 fps and abbreviated for length.

Video S2: **Chiplet Self-aliquoting**. This video focuses on the reaction chambers' filling (slowed by a factor of 10). The video was edited using the Microsoft Clipchamp application.

SECTION S1: PRIMERS SEQUENCE AND AMPLIFICATION DATA

Table S1: The sequences of the primers used in this study

Target	Primer	Sequence
ToBRFV	F3	GTGGTTTTAAGGTGTATAGGTAC
	B3	CTTTCAAATGTGCTCTGATTG
	LF	GAAAGCTCCTAACAAAGCAGTAACT
	LB	ATGACGCAACGGTGGCTAT
	FIP	TCGACTTCTATAATCCTAT-AATGCGGTACTAGATCCTC
	BIP	CGACAACCGCCGAAACGTTA-CAAACCTGTTCCTTTGAC
TMV	F3	GAGTGGAACTTGCCTGAC
	B3	ACAAACTCCAGAGAAAGCG
	LF	CTCGTCGGCTCTTTCCAT
	LB	GCTATAACCACCCAGGACG
	FIP	GCTGCTGTGTAGTAAGATCCGAGTGTGTCTGGTGGACAAA
	BIP	TTTCAGTTCAAGGTCGTTCCCAACTAAAACTTGCCAGACGTT
Tomato (Cox)	F3	TATGGGAGCCGTTTTTGC
	B3	AACTGCTAAGRGCATTCC
	LF	ATGTCCGACCAAAGATTTTACC
	LB	GTATGCCACGTCGCATTCC
	FIP	ATGGATTTGRCCTAAAGTTTCAGGGCAGGATTTCACTATTGGGT
	BIP	TGCATTTCTTAGGGCTTTCGGATCCRGCGTAAGCATCTG

The 1st stage RPA reaction of the Penn-RAMP assay uses the F3 and B3 outer primers, while the 2nd stage LAMP reaction uses F3, B3, LF, LB, FIB, and BIP primers.

Table S2: The sequence of gBlock gene fragments

gBlock*	Sequence
ToBRFV_KT383474_gBlock	TAATACGACTCACTATAGATGTCTTACACAATCGCAACTCC ATCGCAATTTGTGTTTTTGTCATCAGCATGGGCCGACCCT ATAGAATTAATAAATTTATGTACTAATTCACTAGGTAATCA GTTCCAAACACAACAAGCTAGAACAACCGTTCAACGGCAA TTTAGCGAAGTGTGGAAACCTGTCCCTCAAGTCACTGTTA GGTTTCCTGACA**GTGGTTTTAAGGTGTATAGGTACAATG** **CGGTACTAGATCCTCTAGTTACTGCTTTGTTAGGAGCTTT** **CGATACTAGAAATAGGATTATAGAAGTCGAAAATCAGGC** **GAACCCGACAACCGCCGAAACGTTAGACGCTACTCGTA** **GAGTAGATGACGCAACGGTGGCTATAAGGAGCGCTATA** **AATAATTTAGTAGTAGAATTGGTCAAAGGAACAGGTTTG** **TACAATCAGAGCACATTTGAAAG**TGCATCCGGTTTACAAT GGTCCTCTGCACCTGCATCTTGA
TMV_Tor2-L3 gBlock	TAATACGACTCACTATAGTTGCGGAAGATATGTAATACATC ACGACAGAGGATGCATTGTGTATTACGATCCCCTAAAGTT GATCTCGAAACTTGGTGCTAAACACATCAAGGATTGGGAA CACTTGGAGGAGTTCAGAAGGTCTCTTTGTGATGTTGCTG TTTCGTTGAACAATTGTGCGTATTACACACAGTTGGACGA CGCTGTATGGGAGGTTCATAAGACCGCCCCTCCAGGTTC GTTTGTTTATAAAAGTCTGGTGAAGTATTTGTCTGATAAAG TTCTTTTTAGAAGTTTGTTTATAGATGGCTCTAGTTGTTAA AGGAAAAGTGAATATCAATGAGTTTATCGACCTGACAAAA ATGGAGAAGATCTTACCGTCGATGTTTACCCCTGTAAAGA GTGTTATGTGTTCCAAAGTTGATAAAATAATGGTTCATGAG AATGAGTCATTGTCAGGGGTGAACCTTCTTAAAGGAGTTA AGCTTATTGATAGTGGATACGTCTGTTTAGCCGGTTTGGT CGTCACGGGC**GAGTGGAACTTGCCTGACAATTGCAGAG** **GAGGTGTGAGCGTGTGTCTGGTGGACAAAAGGATGGAA** **AGAGCCGACGAGGCCACTCTCGGATCTTACTACACAGC** **AGCTGCAAAGAAAAGATTTCAGTTCAAGGTCGTTCCCAA** **TTATGCTATAACCACCCAGGACGCGATGAAAAACGTCTG** **GCAAGTTTTAGTTAATATTAGAAATGTGAAGATGTCAGC** **GGGTTTCTGTCCGCTTTCTCTGGAGTTTGT**GTCGGTGTGT ATTGTTTATAGAAATAAT

*gBlock gene fragments were used in the study as templates. The bold region represents the amplificon's sequence.

Table S3: The threshold times (min) for benchtop LAMP, benchtop Penn-RAMP, and Penn-RAMP chiplet

Target virus	gBlock Copies/reaction	Threshold time (min) [#]		
		Benchtop LAMP	**Benchtop RAMP**	**Chiplet RAMP**
ToBRFV	5×10^8	8.5 ± 0.1	5.3 ± 0.4	23.0 ± 0.0
	5×10^6	11.1 ± 0.3	6.6 ± 0.3	25.7 ± 0.6
	5×10^4	13.3 ± 0.3	6.6 ± 0.8	26.7 ± 0.6
	5×10^2	14.5 ± 1.8	7.7 ± 0.4	32.0 ± 1.7
	5×10^1	17.3 ± 2.4	7.9 ± 1.0	32.3 ± 0.6
	5×10^0	Negative	9.1 ± 1.3	33.7 ± 0.6
TMV	5×10^8	7.7 ± 0.7	6.0 ± 0.1	27.3 ± 0.6
	5×10^6	9.1 ± 0.1	6.1 ± 0.5	30.3 ± 0.6
	5×10^4	11.3 ± 0.8	6.1 ± 0.2	31.3 ± 0.6
	5×10^2	13.5 ± 0.1	9.0 ± 0.5	34.0 ± 0.0
	5×10^1	18.4 ± 2.3	11.6 ± 1.6	34.3 ± 1.2
	5×10^0	Negative	17.2 ± 0.7	36.7 ± 0.6

[#] The average threshold times (min) and the standard deviation for triplicate assays.

SECTION S2: CHIPLET AND PROCESSOR

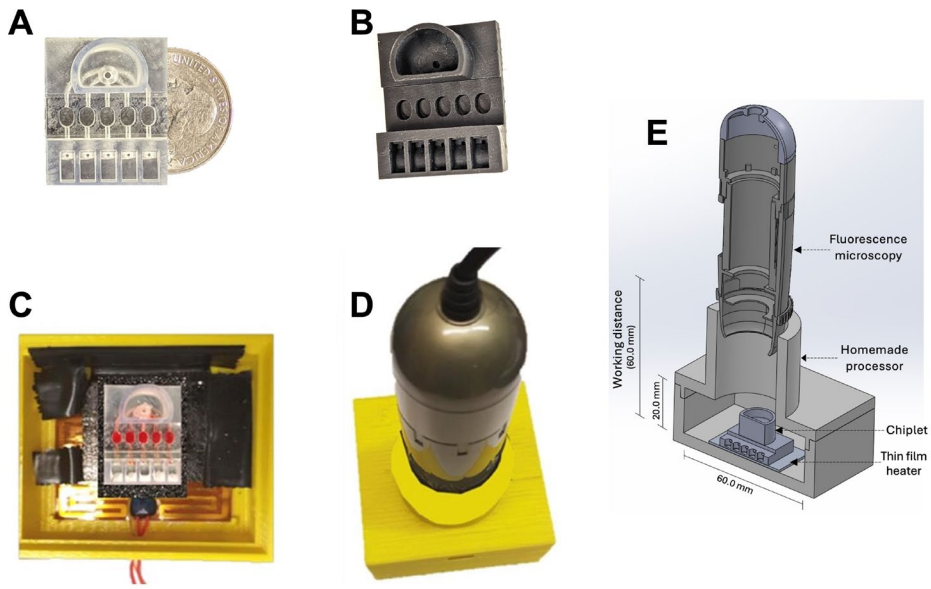

Fig. S1: The 3D - printed chiplet and incubator for the Penn-RAMP assay. (**A**) 3D - printed chiplet made with clear, transparent resin (Formlabs, RS-F2-GPCL-04) for flow visualization and flow-control optimization. A USA quarter dollar coin is included for scale. (**B**) Self-actuated chiplet printed with black resin (Formlabs, RS-F2-GPBK-04). This black chiplet was used for our Penn RAMP assay to minimize background fluorescence. (**C**) Penn-RAMP chiplet placed on a thin film heater with a thermal spreader. (**D**) Our homemade incubator houses a heater, a thermal control circuit board, and a USB fluorescence microscope for real-time image acquisition during Penn-RAMP incubation. (**E**) Cross-section (SOLIDWORKS) of the processor showing the working distance between the camera and the chiplet. Figure not drawn to scale.

SECTION S3: FLOW DISTRIBUTION AND CONTROL

Once the PCM valve (component 7 in Fig. 2C) melts, the first-stage amplification products self-aliquot rapidly by the combined actions of gravity and capillary flow into the second-stage reaction chambers. To image this process, we used a transparent chiplet, phenol red solution [S1] mixed with detergent [S2], and a Google Pixel 7 smartphone camera at 60 frames per second (a video is included as a supplement). This section models this flow process with the Washburn equation [S3]. [1-3]

Fig. S2 depicts a cross-section of our chiplet with one flow conduit and defines the geometric quantities used in our model. L_1, L_2, and L_3, are, respectively, the lengths of the inlet conduit leading into the LAMP reaction chamber, the LAMP reaction chamber, and the exit conduit. *h(t)* is the instantaneous liquid level in the 1st stage reaction chamber, *t* is time, and (*a)* is the length of the vertical descender. We assume that the descender fills nearly instantaneously once the PCM valve melts. We model the process afterward. In section (*0<L<L₁)*, we have the force balance:

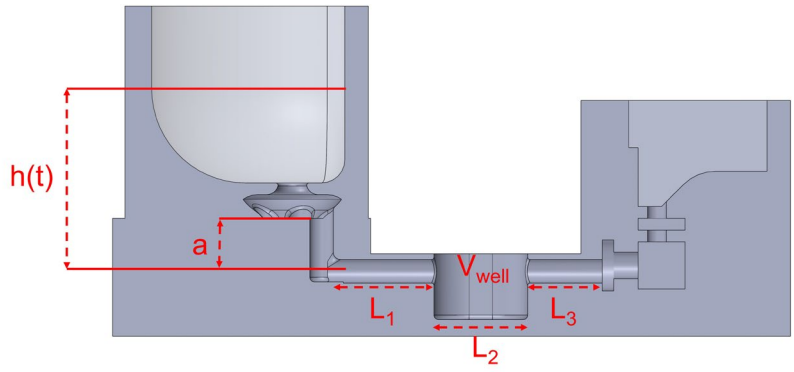

Fig. S2: Vertical cross-section of our chiplet.

$$\left(\rho g(h_{R_0} - 5\frac{A_c}{A_R}L) + \frac{2\,\gamma\,cos\theta}{r}\right)A_c - 2\pi r\tau_{contact} = 8\mu\pi(L+a)\frac{dL}{dt}.\ \ (0 < L < L_1) \qquad \text{(E1)}$$

In the above, the 1st term on the left is the instantaneous pressure head at the inlet, the second is the Laplace pressure deficit behind the advancing meniscus, and the third is contact line resistance. The term on the right is the viscous drag. ρ = *10³ kg m⁻³* is the liquid density, *g* is the gravitational acceleration, A_c is the cross-sectional area of the inlet conduit (*0<L<L₁*) and the exit conduit, A_R is the average cross-sectional area of the 1st stage reaction chamber (approximated as uniform), γ *~30 mN m⁻¹* is the surface tension that accounts for the presence of detergent in the fluid, θ*~47.6°* is the contact angle, *r = 0.5 mm* is the conduit's radius. $\tau_{contact} \sim 10^{-3} N\ m^{-1}$ is the contact line resistance, and μ *~ 6×10⁻³ N m⁻² s* is the liquid viscosity (phenol red with detergent). The 1st stage products are aliquoted into 5 reaction chambers. Thus, the factor "5" in the 1st term on the left. Equation (E1) can be rewritten concisely as:

$$C_1 - C_2 L^* = L^* \frac{dL^*}{dt}, \qquad \text{(E2)}$$

where $C_1 = \frac{1}{8\mu\pi}\left[(A_c \rho g h_{R_0}) + \left(\frac{5A_C^2 \rho g}{A_R} a\right) + \left(A_c \frac{2\,\gamma\, cos\theta}{r}\right) - 2\pi r \tau_{contact}\right]$, $C_2 = \frac{5A_C^2\,\rho g}{8\mu\pi A_R}$, and $L^* = L + a$. We integrate equation (E2) with the initial condition *L*(0)=a* to obtain the implicit relationship between the position (*L*) of the advancing meniscus and time (*t*)

$$t = -\frac{1}{{C_2}^2}\ \left[C_2 L + C_1 ln \frac{C_1 - C_2(L+a)}{C_1 - C_2 a}\right]\ \ (0 < L < L_1,\ \ 0 < t < t_1) \qquad \text{(E3)}$$

When $(L_1 < L < L_1 + L_2)$, the fluid fills the LAMP reaction chamber. In this process, capillary and viscous effects in the LAMP chamber are neglected because of its relatively large cross-sectional area, and the flow is driven by gravity alone until the chamber fills. Equation (E1) reduces to

$$\rho\, g \left(h_{R_1} - 5\frac{A_c}{A_R}\int_{t_1}^{t} u\, dt\right) A_c = 8\mu\pi(L_1 + a)\, u, \qquad \text{(E4)}$$

where *u* is the cross-section averaged fluid velocity. $h_{R_1} = h_{R0} - 5\frac{A_c}{A_R}\big((L_1 + a)\big)$, $\rho\, g A_c h_{R_1} = 8\mu\pi(L_1 + a)\, u(t_1)$, and $A_c \int_{t_1}^{t_2} u\, dt = V_{well}$. Equation (E4) admits the solution

$$u(t) = \frac{(\rho\, g) A_C h_{R_1}}{8\mu\pi(L_1 + a)} e^{-K(t - t_1)}\ \ (t_1 < t < t_2), \qquad \text{(E5)}$$

where $K = \frac{5\,\rho\, g\, {A_C}^2}{8\mu\pi(L_1 + a)A_R}$ and $t_2 - t_1 = -\frac{1}{K}\ln\left(1 - \frac{5\,V_{well}}{A_R h_{R_1}}\right)$.

The flow in the third conduit's segment is like in the first section (E1), accounting for the additional friction associated with the L_1 segment.

$$\left(\rho g (h_{R_2} - 5\frac{A_c}{A_R} l) + \frac{2\,\gamma\, cos\theta}{r}\right) A_c - 2\pi r \tau_{contact} = 8\mu\pi(l + L_1 + a)\frac{dl}{dt}\quad (0 < l < L_3) \qquad \text{(E6)}$$

with $l(t_2)=0$ and $h_{R_2} = h_{R0} - 5\frac{A_c}{A_R}(L_1 + a)$-$5\frac{V_{well}}{A_R}$. Integrating equation (E6), we have

$$t - t_2 = -\frac{1}{{C_4}^2}\ \left[C_4 L + C_3 ln \frac{C_3 - C_4(l + L_1 + a)}{C_3 - C_4(L_1 + a)}\right]\ \ (0 < l < L_3,\ \ t_2 < t < t_3). \qquad \text{(E7)}$$

In the above, $C_3 = \frac{1}{8\mu\pi}\left[(A_c \rho g h_{R_2}) + \left(5A_c \rho g\ \frac{A_c}{A_R}(a + L_1)\right) + \left(A_c \frac{2\,\gamma\, cos\theta}{r}\right) - 2\pi r \tau_{contact}\right]$, $C_4 = \frac{5A_C^2\,\rho g}{8\mu\pi A_R}$, and $t_3 - t_2 = -\frac{1}{{C_4}^2}\ \left[C_4 L_2 + C_3 ln \frac{C_3 - C_4(L_1 + L_3 + a)}{C_3 - C_4(L_1 + a)}\right]$.

Fig. S3 depicts the estimated time as a function of the position of the liquid font. Our experimental data exhibits qualitatively similar behavior, albeit with somewhat slower times, possibly due to the incomplete opening of the phase change valves that restrict the flow.

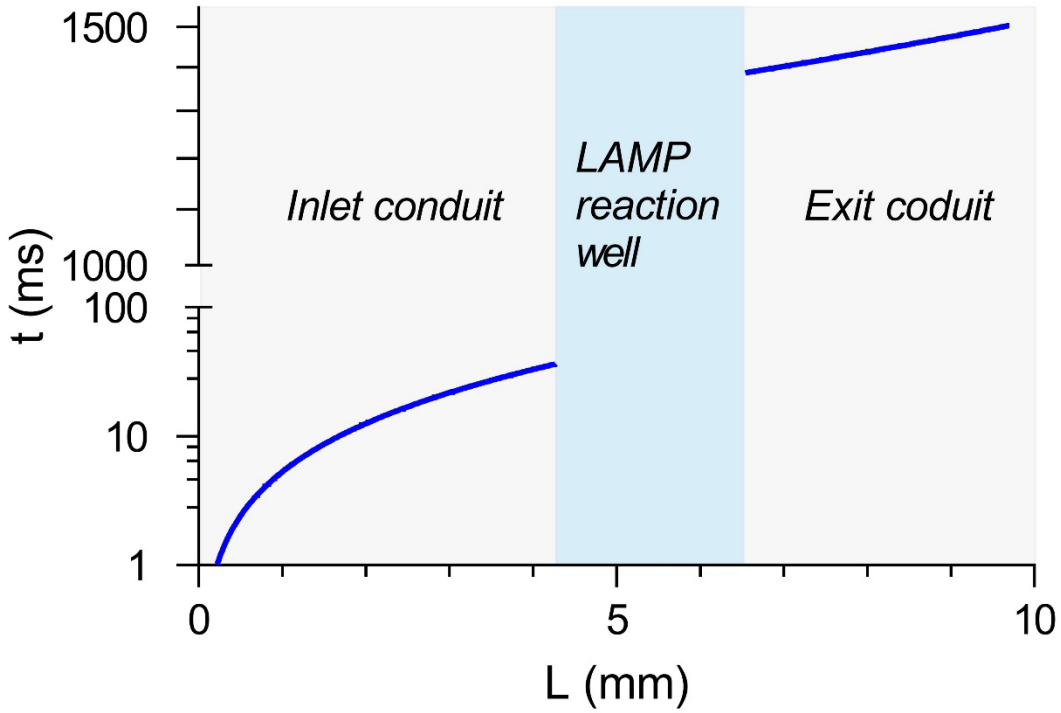

Fig. S3: Time as a function of the liquid front's position during self-aliquoting

When the liquid arrives at the capillary valve (component 4 in Fig. 1A), the meniscus pins and the flow halts. The valve bridging pressure was determined by gradually increasing the height (*h*) of a vertical liquid column of phenol red aqueous solution mixed with 0.1% Tween 20 (to mimic the physiochemical properties of our LAMP reaction mix) in the RPA well upstream of the capillary valve

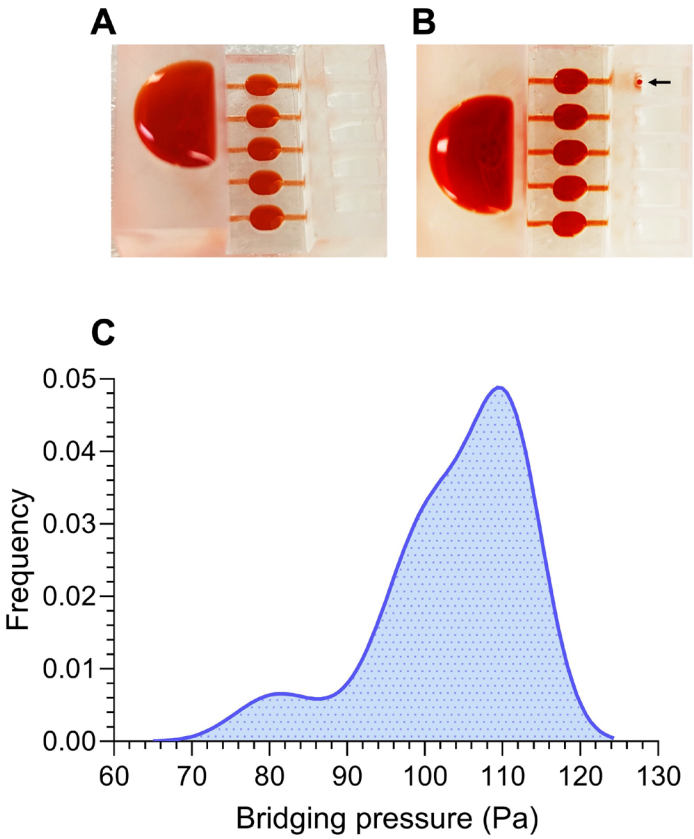

Fig. S4: **Capillarity valve bridging pressure**. When the fluid arrives at the passive valve, the meniscus pins, and the flow halts (**A**). The liquid height (h_C) above which the capillary valve broke (**B**) is the capillary valve bridging pressure $\Delta p_C = \rho\, g\, h_C$ when operating with our reaction buffer, which has surface tension smaller than pure water. In the above, ρ is the liquid density, and g is the gravitational acceleration. (**C**) Kernel density estimation KDE (approximation of the probability density function, *pdf*) of the capillary valve bridging pressure Δp_C. Bridging pressure was estimated using 24 chiplets (N = 24).

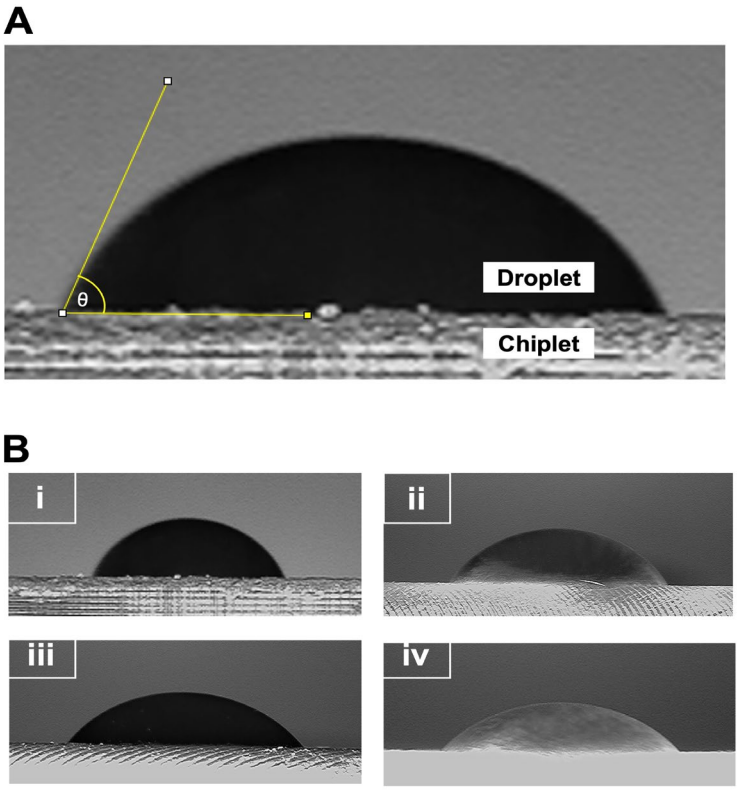

Fig. S5: The wettability of chiplet's material. A droplet (5 µL) of phenol red solution mixed with 0.1% Tween 20 (a surrogate for the reaction buffer) was placed on a flat surface made with the chiplet's resin. (**A**) Enlarged image showing aqueous droplet on the resin surface and the contact angle (*θ*). (**B**) The droplet on clear resin (without PEG treatment) (i), clear resin coated with 2% PEG, black resin (without PEG treatment) (iii), and black resin coated with 2% PEG. The contact angles were determined with ImageJ software and the DropSnake plugin [S4]. The predicted values are in close agreement with direct measurements.

Resin	Coating	Contact angle θ (º)
Clear (Formlabs RS-F2-GPCL-04)	None	67.9 ± 2.8
	PEG	58.5 ± 2.5
Black (Formlabs RS-F2-GPBK-04)	None	50.2 ± 2.1
	PEG	47.6 ± 0.9

#Average contact angle (± standard deviation). All measurements were in triplicate.

SECTION S4: TEMPERATURE DISTRIBUTION

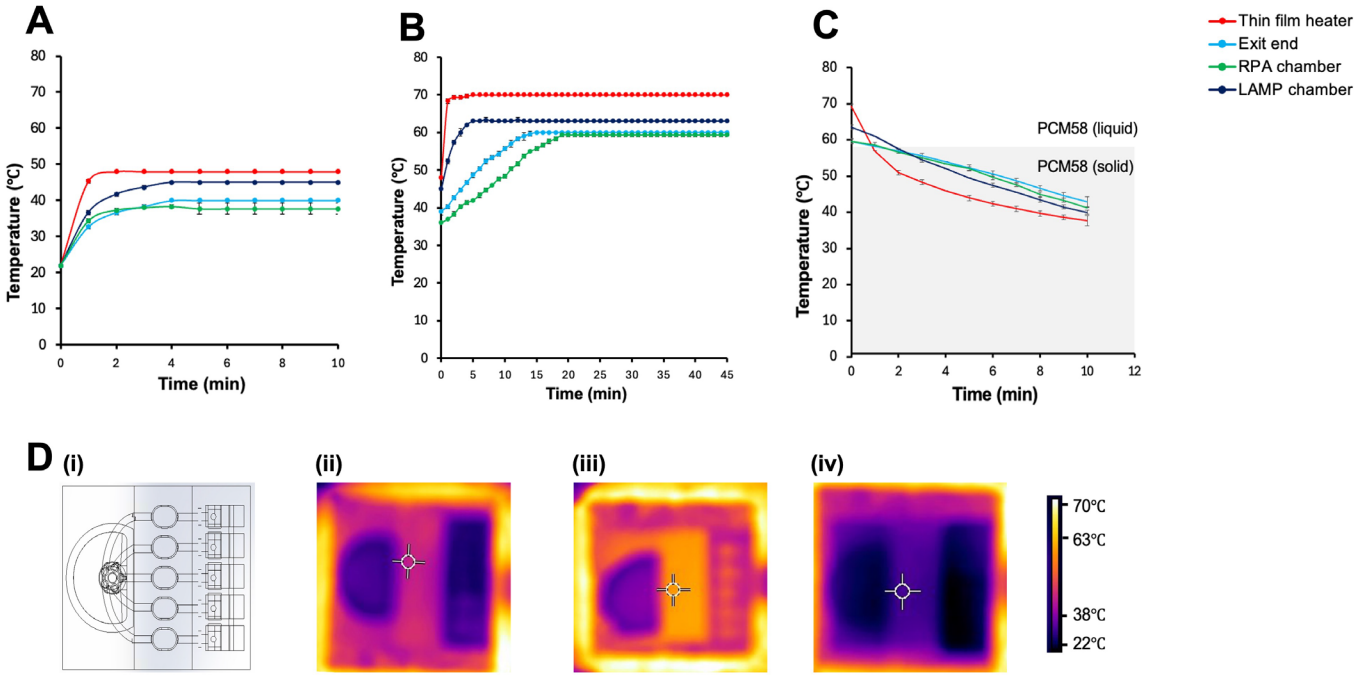

Fig. S6: The temperature of the thin film heater, RPA chamber (inlet), LAMP chamber, and the chiplet's distal end as functions of time during 1st stage RPA incubation (**A**); 2nd stage LAMP reaction (**B)**; and after the power was cut off (**C**). (D) (i) A wireframe top view of the chiplet. Infrared, steady-state thermal images (FLIR E8, TELEDYNE FLIR, USA, https://www.flir.com/support/products/e8/#Overview) of the chiplet during (**ii**)1st stage RPA reaction, (**iii**) 2nd stage LAMP reaction – witness temperature uniformity across the LAMP reaction chambers, and (**iv**) post-RAMP assay. The PCM58 solidifies to seal the inlet and the outlets at <58℃ when the heater is turned off after the RAMP assay. Error bars represent the standard deviation for triplicate measurement.

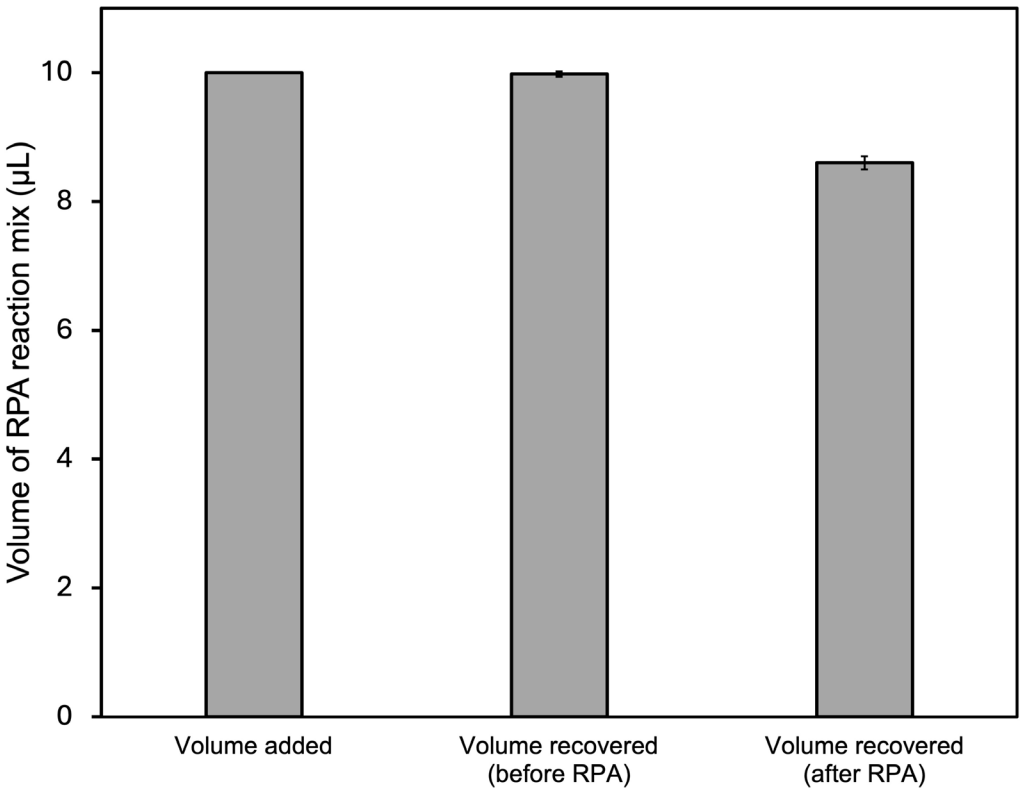

Fig. S7: Volume of the RPA reaction mix added and recovered before and after 10 min incubation at 38ºC. Error bars represent standard deviation. Experiments were carried out in triplicate.

SECTION S5: AMPLIFICATION CURVES

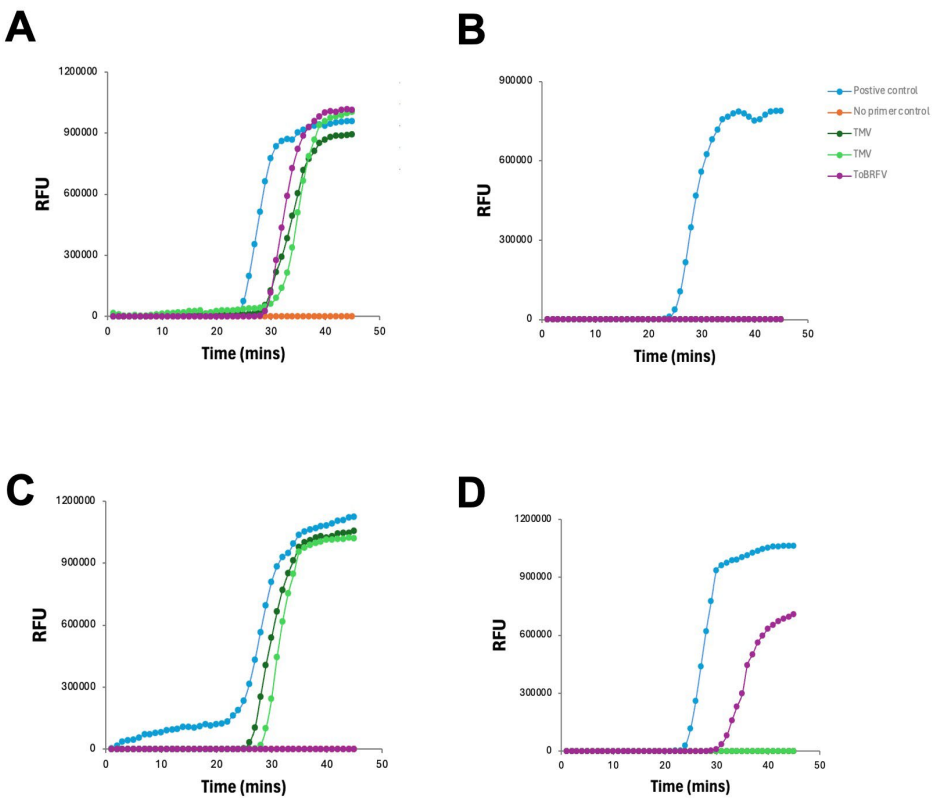

Fig. S8: Amplification curves of tomato viruses nucleic acids carried out on the Penn-RAMP chiplet. Second-stage fluorescent images were processed and analyzed with MATLAB to produce average fluorescent intensity in each reaction chamber as a function of time for samples comprised of (**A**) ToBRFV, TMV, and tomato gDNA; (**B**) only tomato gDNA; (**C**) TMV and tomato gDNA; and (**D**) ToBRFV and tomato gDNA. 10^3 template copies in each reaction. The chiplet was incubated with our homemade processor (**Fig. S1**).

References

[S1] Phenol, https://cameochemicals.noaa.gov/chris/PHN.pdf, (accessed August 2024).

[S2] SIGMA: Tween 20, https://www.sigmaaldrich.com/deepweb/assets/sigmaaldrich/product/documents/217/731/p5927pis.pdf?srsltid=AfmBOooF0J8CcT0GSiNlyRm-8vLFkuZ8yvIoTJX1LZ8XI32JJHyoBCkj, (accessed August 2024).

[S3] É. Ruiz-Gutiérrez, S. Armstrong, S. Lévêque, C. Michel, I. Pagonabarraga, G. G. Wells, A. Hernández-Machado and R. Ledesma-Aguilar, *Journal of Fluid Mechanics*, 2022, **939**, A39.

[S4] Biomedical Imaging Group, Drop shape analysis, https://bigwww.epfl.ch/demo/dropanalysis/ (accessed September 2024)